Biomass Conversion and Biorefinery (2024) 14:14951–14962
https://doi.org/10.1007/s13399-022-03639-y

ORIGINAL ARTICLE

Valorization of olive–pomace as a green sorbent to remove Basic Red 46 (BR46) dye from aqueous solution

Zahra Graba[1] · Imane Akkari[1] · Nacer Bezzi[1] · Mohamed Mehdi Kaci[2]

Received: 12 September 2022 / Revised: 18 November 2022 / Accepted: 5 December 2022 / Published online: 10 December 2022

Abstract

In the current work, a by-product of local olive pomace was valorized as an eco-friendly biosorbent to clear Basic Red 46 dye (BR46). The surface properties of the biosorbent were studied by various analytical implements such as XRF, XRD, FTIR, SEM, and pH_{pzc}. High removal rates (> 90%) were attained at optimal parameters: 240 min of contact, pH of 7, and 400 rpm at 23 °C. The Freundlich model presented the best adjustment of equilibrium curves, while the pseudo-second-order model was the practical kinetic model that matched the experimental data. The results of the thermodynamic investigation revealed that the adsorption process is spontaneous ($\Delta G° < 0$), exothermic $\Delta H°$ (− 40.345 kJ/mol), and probably physical. This study showed that the native olive pomace residue could be successfully transformed into green sorbents of water contaminants.

Keywords Olive pomace by-product · Valorization · Characterization · Adsorption · Dye

1 Introduction

Water, which accounts for almost two-thirds of the earth's surface, is crucial to maintaining life and producing goods in the industrial and agricultural sectors [1]. Nevertheless, due to the growth of industry and urbanization, wastewater dismissal has grown more hazardous, leading to a considerable increase in water pollution [2]. Consequently, the need for clean drinking water has evolved into a problem affecting around 3 billion people [3].

The textile dyeing industry is among the most complicated industrial sectors, characterized by the potential for significant consumption of water, energy, and chemical resources as well as the disposal of enormous volumes of polluted effluent. Many researchers consider it the world's most environmentally polluting industry [4]. Due to their non-biodegradability, carcinogenicity, and mutagenicity, synthetic dyes and their byproducts are among the most toxic effluents, hurting aquatic life, human health, and the environment [5]. Since cationic dyes are some of the most often used dyes in the textile industry, there has been an increased focus on properly administering these dyes in recent years. Basic Red 46 is a kind of azo cationic dye well-known for its chemical stability, which represents better than 10% of all dyes yielded worldwide and is ranked as a harmful organic compound. It also harms aquatic organisms since it impedes the photosynthetic process by decreasing sunlight penetration in water [6]. Before leaving this hazardous pigment in bodies of water, it must first be removed since this might cause harm to the surrounding ecosystem.

Particular focus has been placed on eliminating dyes, with various physical, chemical, and biological procedures used to draw these pervasive contaminants from the environment [7–10]. Even though the processes defined overhead are thriving, they are not viable to employ on a considerable ranking owing to extended working lengths, extreme chemical intake, workforce necessities, heightened costs, and sludge forming, inducing secondary polluting. Given its simple design, ease, effectiveness, ease of operation, environmental, inexpensive pricing,

✉ Imane Akkari
imane.akkari@univ-bejaia.dz

✉ Mohamed Mehdi Kaci
mkaci@usthb.dz

[1] Materials Technology and Process Engineering Laboratory (LTMGP), University of Bejaia, 06000 Bejaia, Algeria

[2] Laboratory of Reaction Engineering, Faculty of Mechanical and Process Engineering (USTHB), BP 32, 16111 Algiers, Algeria

and flexibility, adsorption is becoming an increasingly popular alternative technique for removing dye from textile effluents [11]. Furthermore, several adsorbents, such as biochar prepared from *Chrysanthemum morifolium* Ramat straw [12], Fe@graphite core–shell magnetic nanocomposite [13], and commercial-activated carbon (Norit PK 1–3) [14], have recently been explored for their removal. However, these materials have various limitations due to their high cost and complex production techniques. As a result, it is critical to look for adsorbents with cheap investment costs and a suitable dye removal undertaking.

The biosorption approach, which employs a variety of natural biomass byproduct materials, offers an attractive alternative for solid waste management and dye remediation. For this purpose, numerous bio-based materials have been used lately for adsorptive dye removal, featuring, *Valeriana officinalis* roots, bay leaves (*Laurus nobilis* L.), water tea residue, *Rumex acetosella*, banana, cucumber and potato peels, pomegranate cactus, almond peels, and Judas tree (*Cercis siliquastrum*) seeds [15–23]. Because of the relative abundance and low cost of these biomass materials, as well as their effective dye molecules binding and sequestration potential linked with the abundance of active functional groups on the surface, the biosorption technique seems to be a reliable method for the efficient treatment of dye-polluted wastewaters.

Algeria's Kabylie region is well-known for its olive cultivation, production, and derivatives. One of the most common byproducts with little economic use is olive pomace. However, no prior study has been published that involves the biosorption of Basic Red 46 onto olive pomace. This research aims to use it as a green and cost-effective biosorbent in removing a cationic dye using a simple and effective adsorption approach. The sample was then characterized using various analytical implements, having XRF, XRD, FTIR, SEM, and pH_{pzc}, to remove Basic Red 46. The process's operating parameters are adjusted, whereas the isotherm, kinetic, and thermodynamics are checked. Per this view, this adsorbent can be an alternative exploited for water purification in treatment plants or rural towns.

2 Experimental part

2.1 Dye solution

The cationic dye Basic Red 46 (BR46) is acquired from a nearby textile plant and used immediately without further purification. The primary intention was to create a stock solution (1.0 g/L). Then, it was diluted to the concentrations required for test solutions. Utilizing a pH meter BOECO BT-675, the pH was adjusted with either HCl (0.1 mol/L) or NaOH (0.1 mol/L). Figure 1 depicts the HOMO–LUMO orbitals and molecular electrostatic potential surfaces of BR46 as computed by applying the General Atomic and Molecular Electronic Structure System (GAMESS) software.

2.2 Biosorbent

Initially, olive pomace (OP) was acquired from the discharge of a nearby olive mill. It was then flushed with distilled water, dried for 24 h in an oven at 80 °C, ground in a

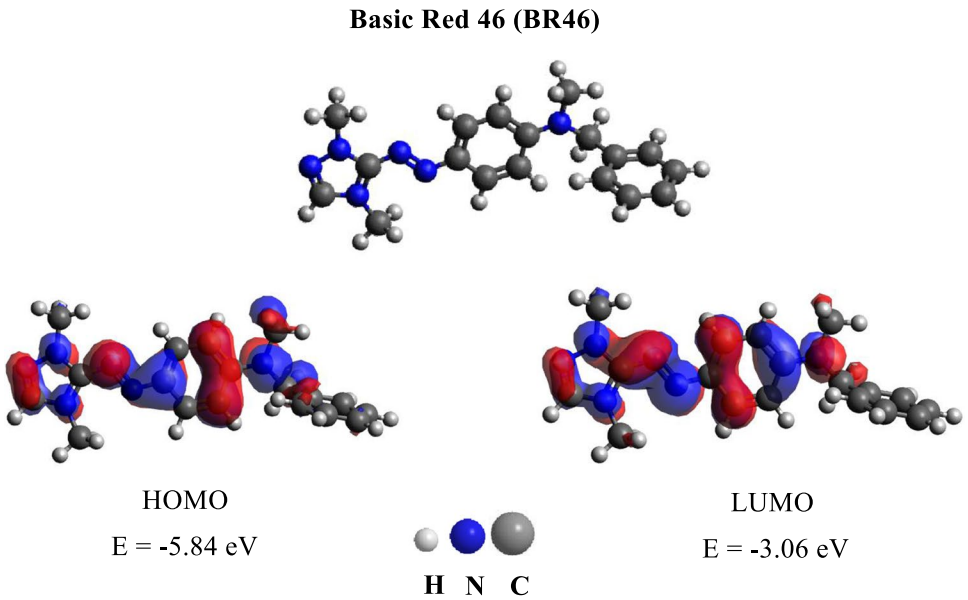

Fig. 1 BR46 dye ($C_{18}H_{21}N_6O_4S$) and its molecular electrostatic potential surfaces and the HOMO–LUMO orbitals

domestic grinder, and sifted into a particle size of 1 mm. The resulting powder was stored in an airtight desiccator receptacle until required.

2.3 Characterization of biosorbent

The elemental constitution of OP was investigated using a Rigaku X-ray Fluorescence Spectrometer "ZSX Primus II." Powder X-ray diffraction (PANalytical Empyrean) was used for the crystallographic research, using a Cu K radiation source (= 0.15418 nm) and a 2θ running from 10 to 80°. The surface chemical groups were qualitatively investigated using Fourier-transform infrared spectroscopy (FTIR). FTIR spectra were obtained using a Nicolet IS5 spectrophotometer (resolution: 0.4 cm^{-1}; a scan rate: 40 $scan.min^{-1}$). The surface morphology was scrutinized using scanning electron microscopy (FEI Quanta 250). Several 50 mL solutions of NaCl (0.01 mol/L) were adjusted in pH from 2 to 12 using NaOH or HCl (0.01 mol/L) to get the pH at the point of zero charges (pH_{pzc}). The mixes were then stirred for 24 h in Erlenmeyer flasks with 0.15 g of OP. Following the conclusion of the stirring time, the pH_{pzc} was determined as the intersection of the results (plotting the pH_{final} vs. $pH_{initial}$ curve) with the bisector.

2.4 Adsorption experiments

Adsorption studies were conducted in batches to examine the effects of various operational factors, including contact duration, OP mass, stirring speed, beginning pH, medium reaction temperature, and initial dye concentration. Isotherms, kinetics, and thermodynamics were also investigated.

Following each test, the systems were centrifuged for 10 min at 6000 rpm. The remaining BR46 concentrations were then measured using a UV–vis spectrophotometer (SHIMADZU UV-1800) at the highest absorption wavelength (λ_{max} = 531 nm).

Calculating the adsorption uptake (q) and removal percentage (R) utilized Eqs. (1) and (2):

$$q_{(e,t)} = \frac{\left(C_0 - C_{(e,t)}\right)V}{M} \tag{1}$$

$$R_{(e,t)} = \frac{\left(C_0 - C_{(e,t)}\right)}{C_0} \times 100 \tag{2}$$

C_0 (mg/L) is the dye concentration at the beginning, C_e and C_t (mg/L) represent, respectively, dye concentrations at the equilibrium and at time t, V (L) is the volume of the solution, and M (g) is the material dried mass.

Several isotherm models featuring Langmuir, Freundlich, and Temkin may be used to study the interactions between BR46 and the OP surface [24–26]. These models are provided in turn in Eqs. (3), (4), and (5):

$$q_e = \frac{q_m K_L C_e}{1 + K_L C_e} \tag{3}$$

$$qe = K_F . C_e^{1/n} \tag{4}$$

$$qe = \mathrm{Bln}(ACe) \tag{5}$$

in which q_e (mg/g) presents the adsorbed quantity at equilibrium, the final adsorbate's concentration is C_e (mg/L), the monolayer adsorption capacity is q_m (mg/g), the Langmuir and Freundlich constants are K_L (L/mg) and K_F, the adsorption intensity is n, A is the Temkin isotherm constant (L/mg) representing maximum binding energy, and B is the Temkin adsorption heat constant (J/mol).

The PFO and PSO kinetic models [27, 28] were investigated to explain the reaction sequence of BR46 adsorption onto OP. Equations (6) and (7) provide these models:

$$q_t = q_e\left(1 - e^{-k_1 t}\right) \tag{6}$$

$$q_t = \frac{k_2 q_e^2 t}{1 + k_2 q_e t} \tag{7}$$

q_t and q_e represent the quantity of BR46 ($mg.g^{-1}$) adsorbed respectively at time and at equilibrium, k_1 represents the PFO rate constant (min^{-1}), and k_2 represents PSO's rate constant (g/mg.min).

The best model fit was evaluated by regression coefficient R-square (R^2), Adj. R-square, and chi-square test (χ^2) [29, 30].

The intraparticle diffusion model was utilized to explore the rate-limiting step of the process [31]; its linear version is provided by Eq. (8):

$$q_t = k_i t^{1/2} + C \tag{8}$$

k_i represents intraparticle diffusion's rate constant (mg/g. min).

The calculation of thermodynamic constants such as $\Delta G°$, $\Delta H°$, and $\Delta S°$ using Eqs. (9) and (10) facilitates understanding of the procedure:

$$\Delta G° = -RTlnK_d \tag{9}$$

$$lnK_d = \frac{\Delta S°}{R} - \frac{\Delta H°}{RT} \quad (10)$$

K_d is the distribution coefficient (q_e/C_e) [32], R represents the universal constant of gasses (~ 8314 J/mol.K), and T (K) represents the absolute temperature.

3 Results and discussion

3.1 Characterization

The major components of agricultural leftovers are cellulose, hemicellulose, and lignin [33]. Their primary constituents are carbon, oxygen, nitrogen, and hydrogen. The elemental makeup of olive pomace by-products is mostly carbon and oxygen, with 26.9% carbon (Table 1).

In general, agricultural leftovers are amorphous [34]. The XRD pattern of OP (Fig. 2) displayed a distinct and broad peak at 2θ = 21°, confirming its amorphous nature.

The OP's FTIR spectrum before adsorption (Fig. 3) shows the following peaks: the prominent peak centered at 3301 cm^{-1} might be caused by stretching vibrations of the OH and NH groups overlapping [35], and at 2922 and 2852 cm^{-1}, the asymmetric stretching vibration of C-H peaks occur [36]. C = O could be linked to the 1629 cm^{-1} peak [37], CN stretching/NH bending modes correspond to the peaks at 1510 and 1244 cm^{-1} [38], and peaks at 1443 and 1033 cm^{-1} are related to C = C and C-O [39]. After adsorption, almost all peaks have shifted positions, revealing that different functional groups on the OP surface could interact with dye molecules.

SEM pictures of OP shown at different magnifications may be seen in Fig. 4 a–d. It is possible to discern an irregular particle form and a rough, heterogeneous, and porous surface, telling that the environment is appropriate for dye molecules to get trapped and adsorbed onto this surface.

In addition, the findings of earlier research [20, 21] have shown that agricultural wastes have a tiny surface area, which is well recognized. However, they function well as adsorbents, implying that adsorption occurs mainly through surface interaction processes [40].

The pH_{pzc} is an excellent tool for determining the adsorbent surface charge. The positive and negative charges on the adsorbent's surface balance when the pH of the solution equals the pH_{pzc}, resulting in an electrically neutral surface. Alternatively, because of the protonation of the surface functional group, the adsorbent surface is generally positively charged in a solution with a pH < pH_{pzc}. Conversely, a solution pH > pH_{pzc} produces a negatively charged surface containing deprotonated functional groups [41]. According to the data given in Table 1, the pH_{pzc} of OP was almost neutral (7.42).

Table 1 Properties of OP

Parameter	Value
C (wt. %)	26.9
O (wt. %)	71.67
Others (wt. %)	1.43
pH_{pzc}	7.42

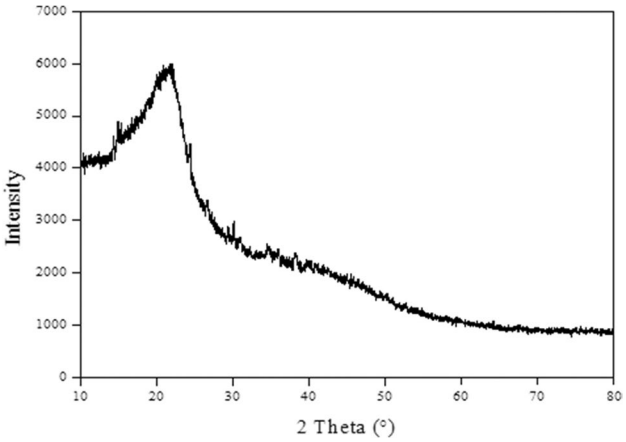

Fig. 2 XRD pattern of OP

3.2 Adsorption parameters

Contact time The aim of studying the influence of contact time on the adsorption process is to select the required duration to establish the adsorption equilibrium. The experiments were conducted out at a temperature of 20 °C, a stirring speed of 500 rpm, an adsorbent mass of

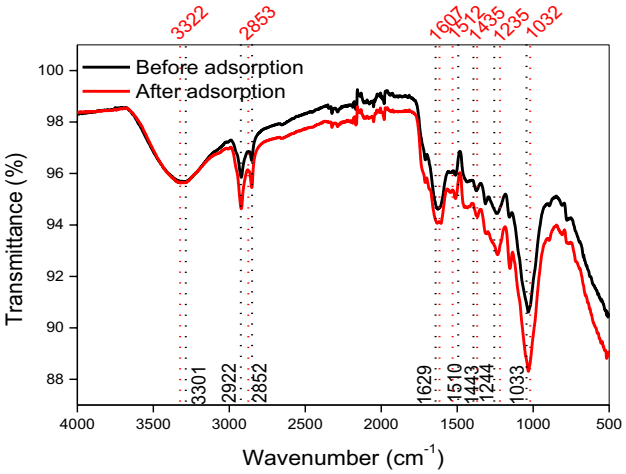

Fig. 3 FTIR spectra of OP before and after adsorption of BR46 dye

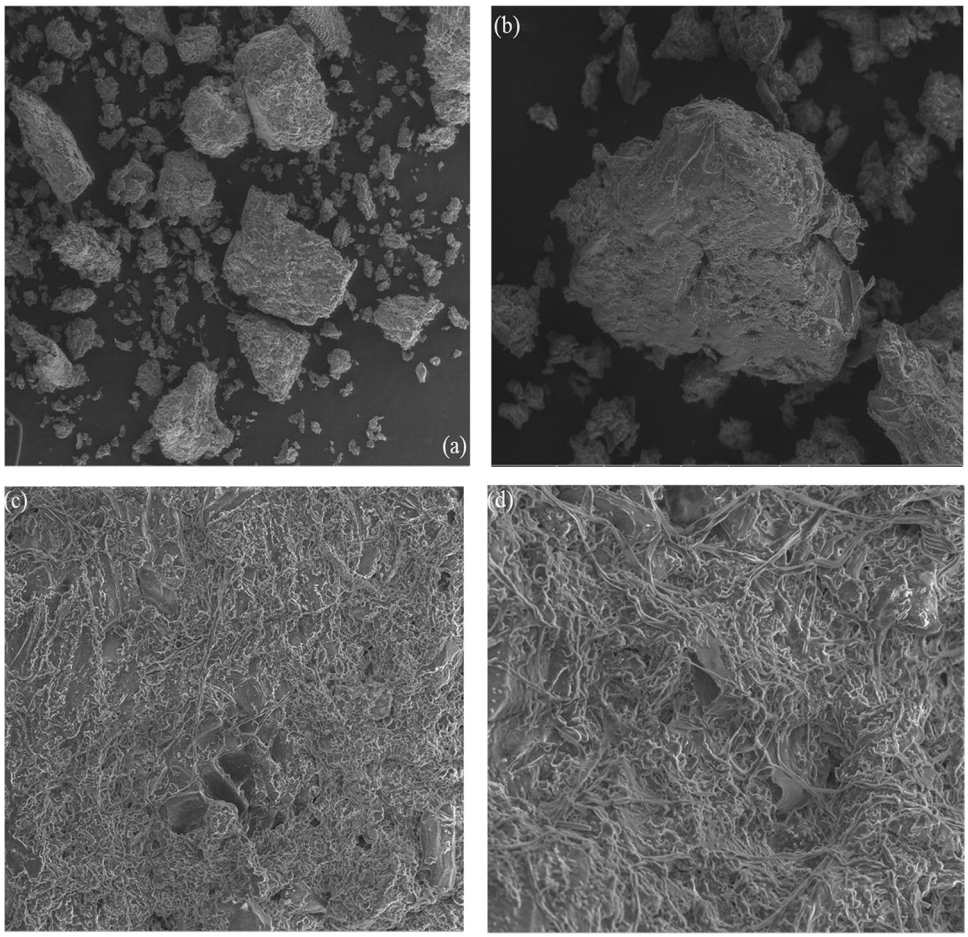

Fig. 4 SEM image of OP at different magnifications (**a**–**d**)

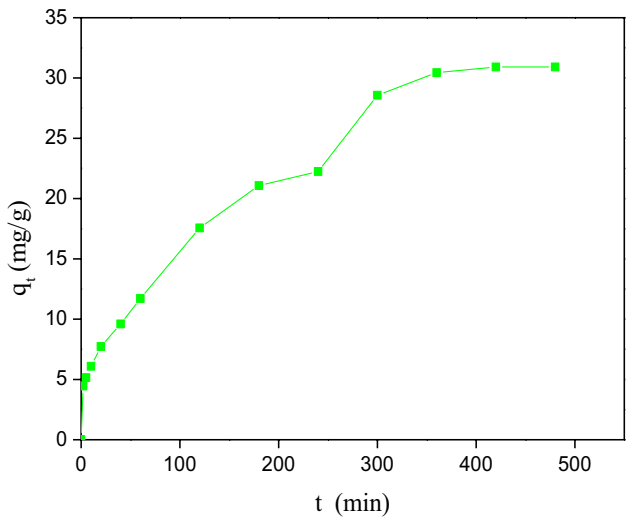

Fig. 5 Effect of contact time

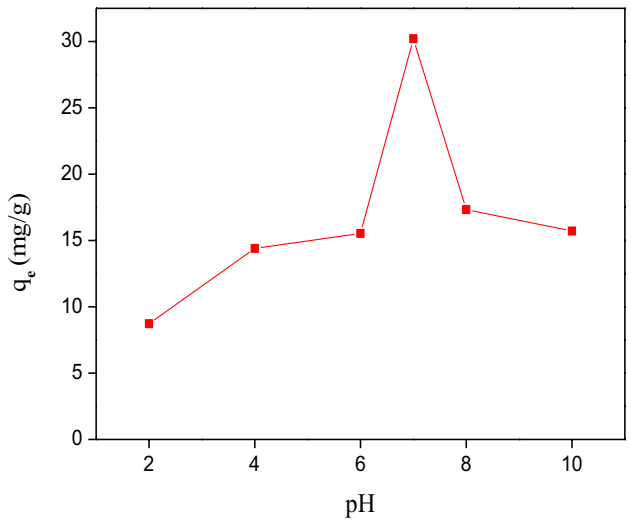

Fig. 6 Effect of solution pH

0.2 g, a pH of 7, and a dye concentration of 200 mg/L. Figure 5 reveals that the adsorption equilibrium is reached after 240 min. The considerable number of active sites readily accessible on the surface of the adsorbent may explain the rapid kinetics seen at the beginning of the reaction during the adsorption phase. As the rate of

surface covering grows, it becomes more challenging to reach the remaining unoccupied spots; as a result, the adsorption rate evolves slowly [42].

Solution pH Since the pH of the solution can influence the surface electrical charges of the adsorbent, the ionization of the dye molecules is likely the most crucial operational parameter in the adsorption process, specifically regarding adsorption capacity. The pH impact (2–10) on BR46 adsorption onto OP is seen in Fig. 6. The adsorption capacity rose from 8.72 (8.53%) to 30.21 mg/g (30.01%) when the pH was raised about 2 to 7, then dropped. For low pH values, the lowering in adsorption capacity may be justified by electrostatic repulsion among the cationic adsorbent surface and the dye molecule's cations, along with a contest for adsorption sites among the hydronium cations and the BR46 cations. Owing to the favorable electrostatic interactions among the anionic adsorbent surface and the cation of the molecule dye, raising the pH improves the adsorption capacity [43]. The electrostatic attraction of hydroxyl anions surrounding the dye cations might be connected to the decline in BR46 retention at higher pHs, which inhibits the dye cations from interacting with the adsorbent anion sites and leads to a drop in BR46 retention.

Biosorbent mass Figure 7 displays the impact of varying OP mass on adsorption performance. The rate of elimination of BR46 increases with increasing OP mass. Indeed, it goes from 1.85 to 94.22% when the mass of OP goes from 0.1 to 6 g, and then it becomes constant. The increase in PO mass leads to an increase in active sites. This results in an increased dye removal rate. When the mass of the biosorbent exceeds a specific value, the yield becomes constant because the addition of biosorbent no longer involves a boost in the accessible surface area of the grains following the formation of agglomerates [44].

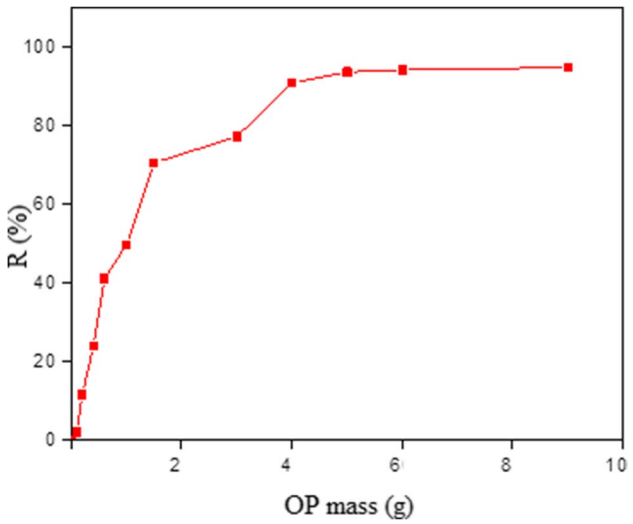

Fig. 7 Effect of biosorbent mass

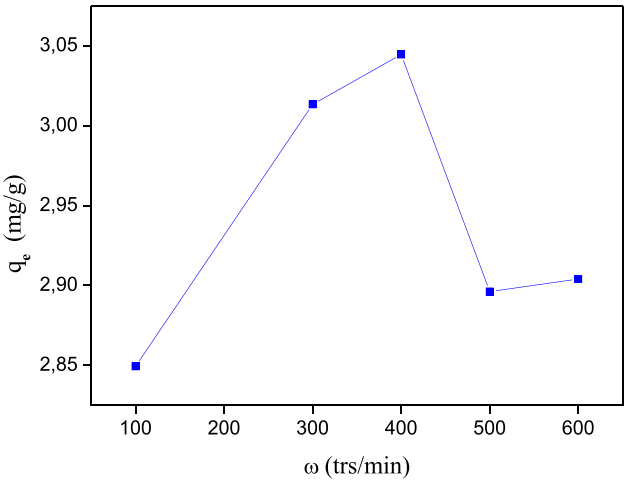

Fig. 8 Effect of agitation speed

Agitation speed Figure 8 shows that the quantity adsorbed at equilibrium increases when the stirring speed *w* increases from 100 to 400 rpm, decreasing considerably. The low amount of dye adsorbed at lower stirring speeds is due to poor dispersion of the OP particles, decreasing the interaction surface between the OP surface and the dye molecules. When the stirring speed is excessively high, more than 400 rpm, giant vortices occur inside the solution, which reduces the adsorbate-biosorbent contact surface [45].

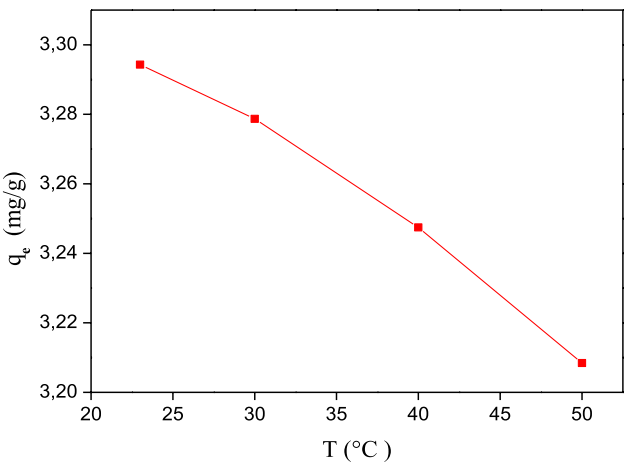

Fig. 9 Effect of temperature

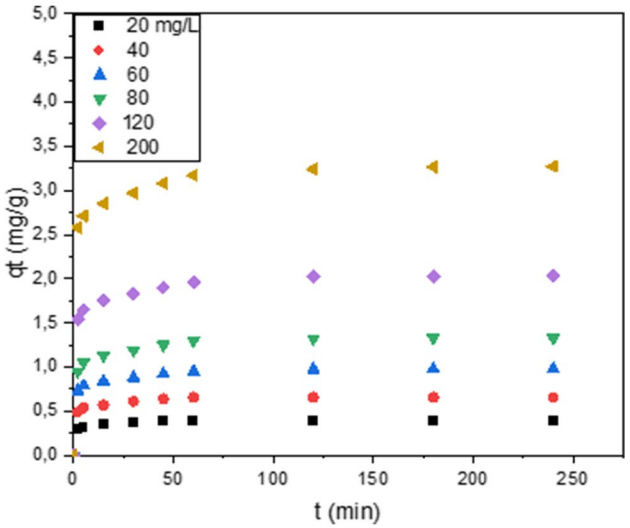

Fig. 10 Effect of initial dye concentration

Table 2 Values of isotherm models' constants

Langmuir	q_m (mg/g)	14.154
	K_L (L/mg)	1.881
	R^2	0.999
	Adj. *R*-square	0.998
	χ^2	0.001
Freundlich	K_F	16.434
	$1/n$	0.862
	n	1.16
	R^2	1
	Adj. *R*-square	1
	χ^2	1.186E-30
Temkin	A (L/mg)	59.533
	B (J/mol)	1.324
	R^2	0.948
	Adj. *R*-square	0.948
	χ^2	0.035

Temperature Adsorption can be an endothermic or exothermic process, leaning on the adsorbent material's nature and the adsorbent molecules. The quantity of BR46 dye removed and the rate at which it is removed decrease as the temperature is elevated (Fig. 9). This decline might result from the adsorbent's active sites being damaged, as well as a reduction in the contact forces between those active sites and the adsorbate [46]. It is also possible that at higher temperatures, species mainly adsorbed on the surface of the adsorbent tend to desorb. The findings point to the possibility that the process will produce exothermic reactions.

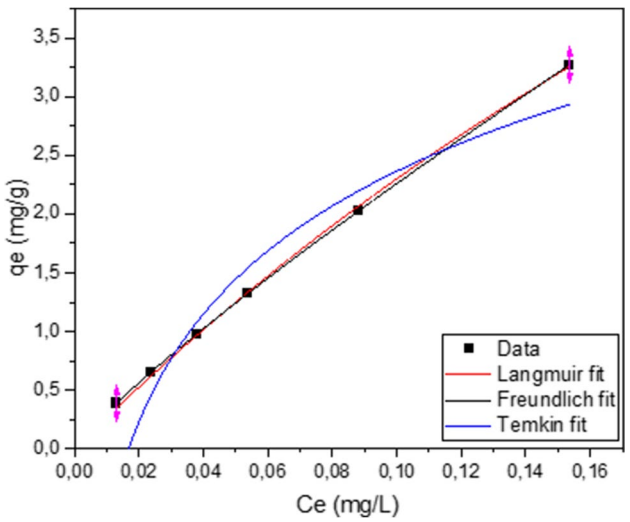

Fig. 11 Non-linear plots of the isotherm models

Initial dye concentration The influence of the initial dye concentration was scrutinized by varying the concentration from 20 to 200 mg/L (Fig. 10). The dye's initial concentration significantly impacts how well the substance absorbs it. As the latter component increases, a higher amount is adsorbed due to a more substantial differential in concentration between BR46 and OP, which increases the driving force required to overcome the mass transfer barrier [47].

3.3 Adsorption isotherms

Figure 11 depicts the non-linear isotherm models' plots. Compared to alternative models, the Freundlich model provides an outstanding fit predicated on R^2, Adj. *R*-square, and χ^2 values (Table 2), indicating that adsorption occurs on a heterogeneous surface with interactions among the deposited BR46 molecules [48]. Furthermore, $1/n$ was $0.862 < 1$ (Table 2), showing that the isotherm is of type L, and the adsorption is spontaneous and favorable [49]. In addition, the heterogeneity factor of the Freundlich model (n) could indicate if the process is linear ($n = 1.0$), chemical ($n < 1.0$), or physical ($n > 1.0$). The value of n was 1.16 suggesting a physical process of adsorption [50].

3.4 Adsorption kinetics

The plots of the non-linear forms of the kinetic models employed are illustrated in Fig. 12, and Table 3 lists the

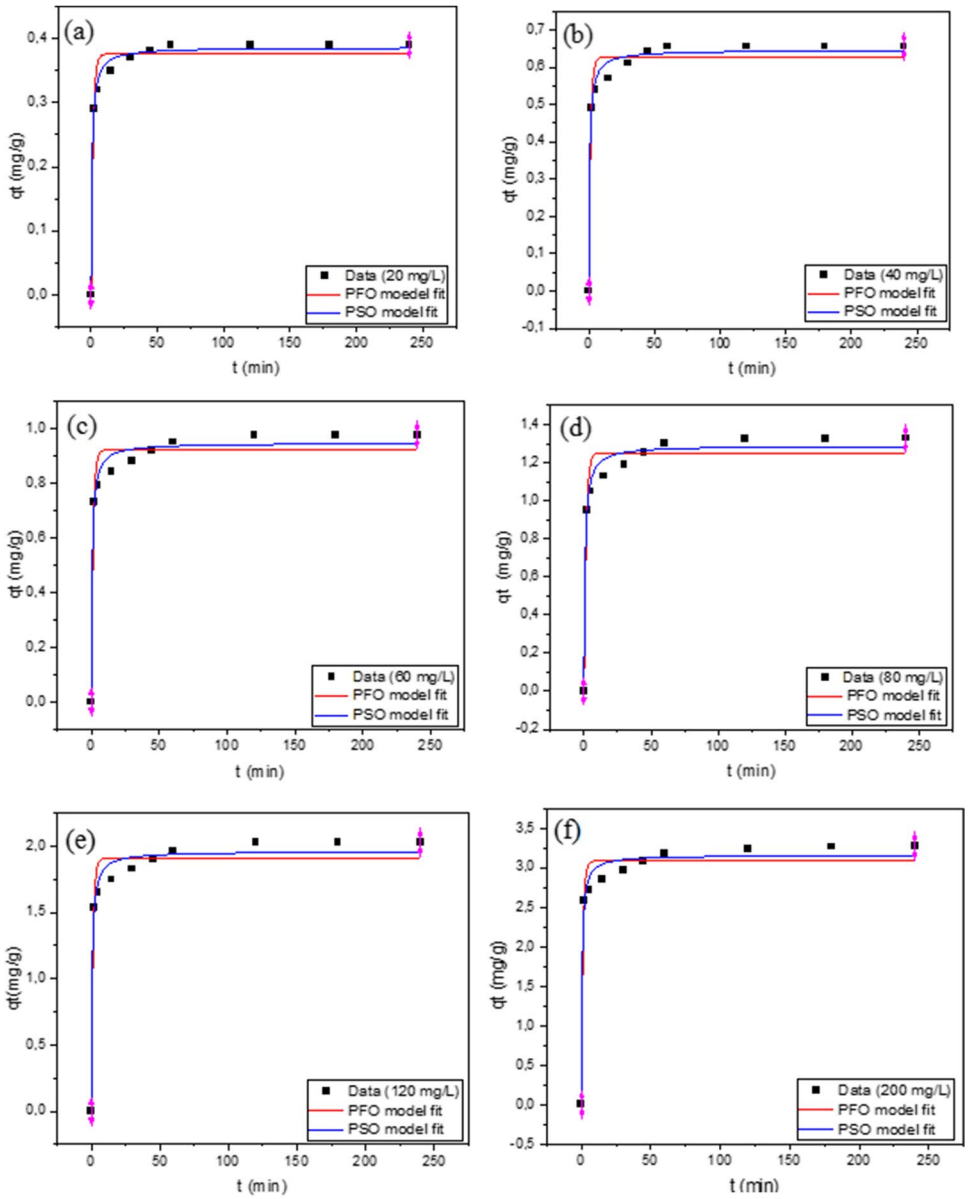

Fig. 12 Non-linear plots of the kinetic models

estimated parameter. The PSO model gives the best fit (higher R^2 and Adj. R-square values with the lower χ^2 values). In addition to that, the experimental and calculated adsorption capacities using this model are closer, suggesting that PSO kinetic model describes the process better. These results indicate that chemisorption occurs in addition to multilayer physical interactions discussed in the isotherm study [51].

The results of the intraparticle diffusion model are given in Fig. 13 and Table 4. In its most general form, the intraparticle diffusion model is represented by three straight-line sections with varying slopes. The steep section is the phase in which the solute and solution move toward the adsorbent's outer edge coating as a result of external surface adsorption (k_1). When a straight line travels through the origin at the rate-limiting stage, the boundary layer control is bypassed, allowing for complete pore diffusion. The gradual section, on the other hand, refers to the solute gradually spreading onto the adsorbent (k_2). Finally, the stable section denotes the

Table 3 Kinetic parameters

Concentration (mg/L)	$q_{e\,exp}$ (mg/g)	Pseudo first-order model					Pseudo second-order model				
		$q_{e\,cal}$ (mg/g)	k_1 (min^{-1})	R^2	Adj. R-square	χ^2	$q_{e\,cal}$ (mg/g)	k_2 (g/mg.min)	R^2	Adj. R-square	χ^2
20	0.390	0.375	0.660	0.973	0.969		0.386	3.332	0.993	0.992	1.064E-4
40	0.656	0.627	0.685	0.967		4.367E-4	0.645	2.047	0.988	0.987	5.173E-4
60	0.976	0.919	0.715	0.961	0.962	0.001	0.945	1.451	0.984	0.982	0.001
80	1.327	1.249	0.629	0.957	0.957	0.003	1.288	0.887	0.984	0.982	0.002
120	2.029	1.908	0.751	0.962	0.952	0.007	1.960	0.750	0.981	0.981	0.006
200	3.270	3.082	0.846	0.9679	0.957	0.015	3.157	0.564	0.985	0.983	0.015
					0.963	0.034					

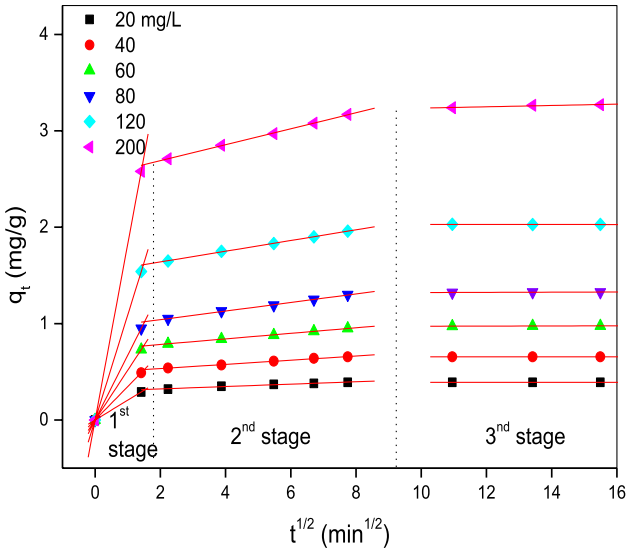

Fig. 13 Plot of intraparticle diffuion model

point where adsorption approaches equilibrium, and the residual solute in the solution is so small that it slows the spread (k_3) [52]. Figure 13 and Table 4 show areas with a slight slope and flat sections, implying that border movement outside the adsorbent was instantaneous [53]. Rather, at the rate-limiting step, intraparticle diffusion took place [54].

3.5 Thermodynamic study and general discussion

The values of $\Delta H°$ and $\Delta S°$ may be computed using the slope and intercept of the plot ln K_d against $1/T$ (Fig. 14). These values are then used to describe the spontaneity, sorption heat, and randomness at the adsorbent-solution interface (Table 5). The negative value $\Delta G°$ implies that the process is spontaneous, while the negative value of $\Delta H°$ (− 40.345 kJ/mol) indicates that the process is exothermic; this matter is in the scope of 1–60 kJ/mol, meaning that the process might be regulated by physical sorption [55]. Furthermore, the negative value of $\Delta S°$ (− 0.132 kJ/mol.K) implies that the randomness at the solid–liquid interface has decreased.

To summarize, the adsorption mechanism could be managed by chemisorption in addition to multilayer physical sorption, including electrostatic interactions and intraparticle diffusion at the rate-limiting step, according to the obtained results.

In comparison to some adsorbents reported in the literature (Table 6), OP has an average adsorption capacity of 14.15 mg/g with high removal rates (> 90%). However, this biosorbent is green, inexpensive, and requires

Table 4 Intraparticle diffusion rate constants

Concentration (mg/L)	Intraparticle diffusion rate constants (mg/g.min)					
	k_1	R^2	k_2	R^2	k_3	R^2
20	0.205	1	0.012	0.986	0	-
40	0.346	1	0.021	0.997	0	-
60	0.516	1	0.028	0.999	6.782E-4	0.889
80	0.671	1	0.044	0.999	8.919E-4	0.973
120	1.088	1	0.055	0.999	0	-
200	1.824	1	0.082	0.999	0.006	0.949

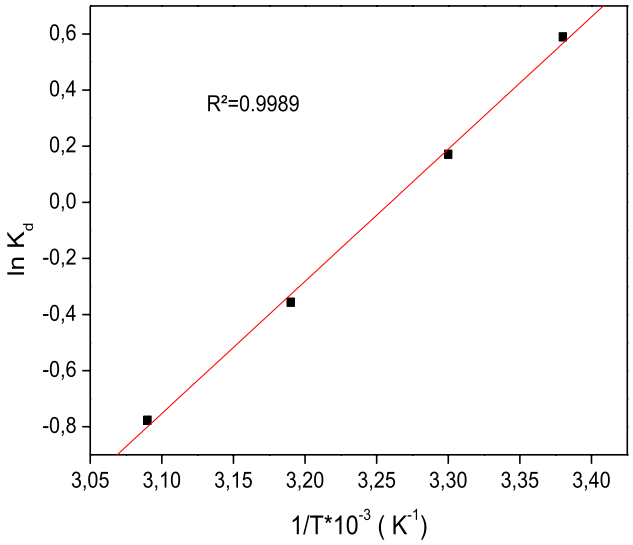

Fig. 14 Plot of the Van't Hoff equation

no chemical or physical modification, whereas others could be relatively expensive and could require complex preparation procedures, large volumes of chemicals, and high energies, making OP suitable for the biosorption of pollutants in liquid media.

Table 5 Thermodynamic parameters at different temperatures

T (K)	$\Delta G°$ (kJ/mol)	$\Delta H°$ (kJ/mol)	$\Delta S°$ (kJ/mol.K)
296.15	− 1.393	− 40.345	− 0.132
303.15	− 0.473		
313.15	0.842		
323.15	0.258		

4 Conclusion

This work investigated the by-product of olive pomace (OP) as a cost-effective biosorbent to remove BR46 dye. The physicochemical properties of OP were described using XRF, XRD, FTIR, SEM, and pH_{pzc}. The results show that its surface is amorphous, rough, heterogeneous and rich in functional groups, making it an ideal environment for pollutant molecules to be trapped. Adsorption studies were performed in a batch system, and operational factors such as contact duration, solution pH, OP mass, agitation speed, temperature, and starting BR46 concentration were investigated, resulting in high removal rates (> 90%). The Freundlich and the pseudo-second-order models were used to provide the data for the isotherm and the kinetics, respectively. The thermodynamic investigation meant that the adsorption process is spontaneous ($\Delta G° < 0$), exothermic $\Delta H°$ (− 40.345 kJ/mol), and most likely physical. In summary, our study implies that the by-product of olive pomace could be developed into a cost-effective and green alternative to remove persisting organic toxins, including the cationic dye BR46.

Table 6 Comparison of BR46 dye adsorption

Adsorbent	Adsorption capacity (mg. g^{-1})	Reference
Biochar prepared from *Chrysanthemum morifolium* Ramat straw	53.19	[12]
Fe@graphite core–shell magnetic nanocomposite	46.7	[13]
Commercial-activated carbon (Norit PK 1–3)	50.78	[14]
Olive pomace	14.15	This study

Acknowledgements The authors would like to thank the Algerian Ministry of High Education and the University of Bejaia for the financial support.

Author contribution Zahra Graba, Imane Akkari, Nacer Bezzi, and Mohamed Mehdi Kaci: conceptualization, interpretation of results, writing, and editing.

Data availability Not applicable.

Declarations

Ethical approval Not applicable.

Consent to participate Not applicable.

Consent for publication Not applicable.

Competing interests The authors declare no competing interests.

References

1. Hu H, Al-Ghamdi AA, Yang S, Tian Z, Cheng B, Ho W (2020) NiFe-LDH nanosheet/carbon fiber nanocomposite with enhanced anionic dye adsorption performance. Appl Surf Sci 511:145570
2. Saxena M, Sharma N, Saxena R (2020) Highly efficient and rapid removal of a toxic dye: adsorption kinetics, isotherm, and mechanism studies on functionalized multiwalled carbon nanotubes. Surface and Interfaces 21:100639
3. Mansor ES, Ali H, Abdel-Karim A (2020) Efficient and reusable polyethylene oxide/polyaniline composite membrane for dye adsorption and filtration. Colloid Interface Sci Commu 39:100314
4. Berkessa YW, Yan B, Li T, Jegatheesan V, Zhang Y (2020) Treatment of anthraquinone dye textile wastewater using anaerobic dynamic membrane bioreactor: performance and microbial dynamics. Chemosphere 238:124539
5. Akkari I, Graba Z, Bezzi N, Kaci MM, Merzeg FA, Bait N, ... , Benguerba Y (2022) Effective removal of cationic dye on activated carbon made from cactus fruit peels: a combined experimental and theoretical study. Environ Sci Pollut Res 1–18.
6. Kaci MM, Nasrallah N, Atmani F, Kebir M, Guernanou R, Soukeur A, Trari M (2021) Enhanced photocatalytic performance of $CuAl_2O_4$ nanoparticles spinel for dye degradation under visible light. Res Chem Intermed 47(9):3785–3806
7. Jain P, Bhavani AG, Singh P, Singh MB (2022) Fundamental of aerobic and anaerobic processes in dye wastewater. In Biological Approaches in Dye-Containing Wastewater (pp. 39–55). Springer, Singapore
8. Kaci MM, Nasrallah N, Djaballah AM, Akkari I, Belabed C, Soukeur, Atmani F, Trari M (2022) Insights into the optical and electrochemical features of $CuAl_2O_4$ nanoparticles and it use for methyl violet oxidation under sunlight exposure. Optical Materials 126 112198
9. Atmani F, Kaci MM, Yeddou-Mezenner N, Soukeur A, Akkari I, Navio JA (2022) Insights into the physicochemical properties of sugar scum as a sustainable biosorbent derived from sugar refinery waste for efficient cationic dye removal. Biomass Convers Biorefin 1–15
10. Arefi-Oskoui S, Khataee A, Behrouz SJ, Vatanpour V, Gharamaleki SH, Orooji Y, Safarpour M (2022) Development of MoS2/O-MWCNTs/PES blended membrane for efficient removal of dyes, antibiotic, and protein. Sep Purif Technol 280:119822
11. Graba Z, Hamoudi S, Bekka D, Bezzi N, Boukherroub R (2015) Influence of adsorption parameters of basic red dye 46 by the rough and treated Algerian natural phosphates. J Ind Eng Chem 25:229–238
12. Yang X, Zhu W, Song Y, Zhuang H, Tang H (2021) Removal of cationic dye BR46 by biochar prepared from Chrysanthemum morifolium Ramat straw: a study on adsorption equilibrium, kinetics and isotherm. J Mol Liq 340:116617
13. Konicki W, Hełminiak A, Arabczyk W, Mijowska E (2018) Adsorption of cationic dyes onto Fe@ graphite core–shell magnetic nanocomposite: Equilibrium, kinetics and thermodynamics. Chem Eng Res Des 129:259–270
14. Senoussi H, Bouhidel KE (2018) Feasibility and optimisation of a batch mode capacitive deionization (BM CDI) process for textile cationic dyes (TCD) removal and recovery from industrial wastewaters. J Clean Prod 205:721–727
15. Akdemir M, Isik B, Cakar F, Cankurtaran O (2022) Comparison of the adsorption efficiency of cationic (Crystal Violet) and anionic (Congo Red) dyes on Valeriana officinalis roots: isotherms, kinetics, thermodynamic studies, and error functions. Mater Chem Phys 291:126763
16. Isik B, Avci S, Cakar F, Cankurtaran O (2022) Adsorptive removal of hazardous dye (crystal violet) using bay leaves (Laurus nobilis L.): surface characterization, batch adsorption studies, and statistical analysis. Environ Sci Pollut Res 1–24
17. Jain SN, Tamboli SR, Sutar DS, Jadhav SR, Marathe JV, Shaikh AA, Prajapati AA (2020) Batch and continuous studies for adsorption of anionic dye onto waste tea residue: kinetic, equilibrium, breakthrough and reusability studies. J Clean Prod 252:119778
18. Erdogan Y, Isik B, Ugraskan V, Cakar F (2022) Effective and fast removal of crystal violet dye from aqueous solutions using Rumex acetosella: isotherm, kinetic, thermodynamic studies, and statistical analysis. Biomass Convers Biorefin 1–16
19. Stavrinou A, Aggelopoulos CA, Tsakiroglou CD (2018) Exploring the adsorption mechanisms of cationic and anionic dyes onto agricultural waste peels of banana, cucumber and potato: adsorption kinetics and equilibrium isotherms as a tool. J Environ Chem Eng 6(6):6958–6970
20. Akkari I, Graba Z, Bezzi N, Merzeg FA, Bait N, Ferhati A (2021). Raw pomegranate peel as promise efficient biosorbent for the removal of Basic Red 46 dye: equilibrium, kinetic, and thermodynamic studies. Biomass Convers Biorefin 1–14
21. Akkari I, Graba Z, Bezzi N, Merzeg FA, Bait N, Ferhati A, Kaci MM (2022) Biosorption of Basic Red 46 using raw cactus fruit peels: equilibrium, kinetic and thermodynamic studies. Biomass Convers Biorefin 1–12
22. Al-Musawi TJ, Arghavan SMA, Allahyari E, Arghavan FS, Othmani A, Nasseh N (2022) Adsorption of malachite green dye onto almond peel waste: a study focusing on application of the ANN approach for optimization of the effect of environmental parameters. Biomass Convers Biorefin 1–12
23. Isik B, Ugraskan V, Cakar F, Yazici O (2022). A comparative study on the adsorption of toxic cationic dyes by Judas tree (Cercis siliquastrum) seeds. Biomass Convers Biorefin 1–15
24. Langmuir I (1918) The adsorption of gases on plane surfaces of glass, mica and platinum. J Am Chem Soc 40(9):1361–1403
25. Freundlich HMF (1906) Over the adsorption in solution. J Phys chem 57(385471):1100–1107
26. Temkin MJ, Pyzhev V (1940) Recent modifications to Langmuir isotherms.
27. Lagergren SK (1898) About the theory of so-called adsorption of soluble substances. Sven Vetenskapsakad Handingarl 24:1–39
28. Ho YS, McKay G (1999) Pseudo-second order model for sorption processes. Process Biochem 34(5):451–465
29. Bagdonavicius V, Nikulin MS (2011) Chi-squared goodness-of-fit test for right censored data. The Int J App Mathematics Statistics 24(1):1–11
30. Guedidi H, Reinert L, Soneda Y, Bellakhal N, Duclaux L (2017) Adsorption of ibuprofen from aqueous solution on

chemically surface-modified activated carbon cloths. Arab J Chem 10:S3584–S3594
31. Weber WJ Jr, Morris JC (1963) Kinetics of adsorption on carbon from solution. J Sanit Eng Div 89(2):31–59
32. Nasrullah A, Bhat AH, Naeem A, Isa MH, Danish M (2018) High surface area mesoporous activated carbon-alginate beads for efficient removal of methylene blue. Int J Biol Macromol 107:1792–1799
33. Thakur V, Sharma E, Guleria A, Sangar S, Singh K (2020) Modification and management of lignocellulosic waste as an ecofriendly biosorbent for the application of heavy metal ions sorption. Materials Today: Proceedings 32:608–619
34. de O Salomón, YL, Georgin, J, Dos Reis, GS, Lima, ÉC, Oliveira, ML, Franco, DS., ... & Dotto, G. L. (2020). Utilization of Pacara Earpod tree (Enterolobium contortisilquum) and Ironwood (Caesalpinia leiostachya) seeds as low-cost biosorbents for removal of basic fuchsin. Environmental Science and Pollution Research, 27(26), 33307-33320
35. Mokhtar N, Aziz EA, Aris A, Ishak WFW, Ali NSM (2017) Biosorption of azo-dye using marine macro-alga of EuchemaSpinosum. J Environ Chem Eng 5(6):5721–5731
36. Niazi L, Lashanizadegan A, Sharififard H (2018) Chestnut oak shells activated carbon: preparation, characterization and application for Cr (VI) removal from dilute aqueous solutions. J Clean Prod 185:554–561
37. Li Z, Hanafy H, Zhang L, Sellaoui L, Netto MS, Oliveira ML, ... Li Q (2020) Adsorption of congo red and methylene blue dyes on an ashitaba waste and a walnut shell-based activated carbon from aqueous solutions: experiments, characterization and physical interpretations. J Chem Eng 388, 124263
38. Baláž M, Ficeriová J, Briančin J (2016) Influence of milling on the adsorption ability of eggshell waste. Chemosphere 146:458–471
39. Li Y, Wang A, Bai Y, Wang S (2017) Evaluation of a mixed anionic–nonionic surfactant modified eggshell membrane as an advantageous adsorbent for the solid-phase extraction of Sudan I-IV as model analytes. J Sep Sci 40(12):2591–2602
40. Omorogie MO, Babalola JO, Unuabonah EI, Song W, Gong JR (2016) Efficient chromium abstraction from aqueous solution using a low-cost biosorbent: Naucleadiderrichii seed biomass waste. J Saudi Chem Soc 20(1):49–57
41. Liu ZF, Liu ZJ, Qie LM, Yao ZY (2021) Effects of melanin extraction on biosorption behavior of chestnut shells towards methylene blue. Water Conserv Sci Eng 6(3):163–173
42. Jiang D, Yang Y, Huang C, Huang M, Chen J, Rao T, Ran X (2019) Removal of the heavy metal ion nickel (II) via an adsorption method using flower globular magnesium hydroxide. J Hazard Mater 373:131–140
43. Naushad M, Alqadami AA, AlOthman ZA, Alsohaimi IH, Algamdi MS, Aldawsari AM (2019) Adsorption kinetics, isotherm and reusability studies for the removal of cationic dye from aqueous medium using arginine modified activated carbon. J Mol Liq 293:111442
44. Mandal A, Bar N, Das SK (2020) Phenol removal from wastewater using low-cost natural bioadsorbent neem (Azadirachta indica) leaves: adsorption study and MLR modeling. Sustainable Chem Pharmacy 17:100308
45. Akkari I, Graba Z, Bezzi N, Vithanage M, Kaci MM (2022) New insights into the effective removal of Basic Red 46 onto activated carbon produced from pomegranate peels. Biomass Convers Biorefin 1–14.
46. Deniz F, Saygideger SD (2011) Removal of a hazardous azo dye (Basic Red 46) from aqueous solution by princess tree leaf. Desalination 268(1–3):6–11
47. Shabaan OA, Jahin HS, Mohamed GG (2020) Removal of anionic and cationic dyes from wastewater by adsorption using multiwall carbon nanotubes. Arab J Chem 13(3):4797–4810
48. Al-Trawneh SA, Jiries AG, Alshahateet SF, Sagadevan S (2021) Phenol removal from aqueous solution using synthetic V-shaped organic adsorbent: kinetics, isotherm, and thermodynamics studies. Chem Phys Lett 781:138959
49. Rambabu K, Bharath G, Banat F, Show PL (2020) Biosorption performance of date palm empty fruit bunch wastes for toxic hexavalent chromium removal. Environ Res 187:109694
50. Zanella HG, Spessato L, Lopes GK, Yokoyama JT, Silva MC, Souza PS, ... Almeida VC (2021). Caffeine adsorption on activated biochar derived from macrophytes (Eichornia crassipes). J Mol Liq 340, 117206
51. Beltrame KK, Cazetta AL, de Souza PS, Spessato L, Silva TL, Almeida VC (2018) Adsorption of caffeine on mesoporous activated carbon fibers prepared from pineapple plant leaves. Ecotoxicol Environ Saf 147:64–71
52. Cheung WH, Szeto YS, McKay G (2007) Intraparticle diffusion processes during acid dye adsorption onto chitosan. Biores Technol 98(15):2897–2904
53. Shin HS, Kim JH (2016) Isotherm, kinetic and thermodynamic characteristics of adsorption of paclitaxel onto Diaion HP-20. Process Biochem 51(7):917–924
54. Kim YS, Kim JH (2019) Isotherm, kinetic and thermodynamic studies on the adsorption of paclitaxel onto Sylopute. J Chem Thermodyn 130:104–113
55. Miyah Y, Lahrichi A, Idrissi M, Khalil A, Zerrouq F (2018) Adsorption of methylene blue dye from aqueous solutions onto walnut shells powder: equilibrium and kinetic studies. Surfaces and Interfaces 11:74–81